# 4

# Hydrodynamic motion

## 4.1 Derivation of Navier–Stokes equations

### *4.1.1 Continuum flux*

Our goal in this chapter is to provide a complete mathematical description of plasmas in motion, and to describe how the motion changes with time in response to applied forces. The equations of motion are the central and most essential part of all simulation computer codes. All the other physical processes operative in matter at extreme conditions – thermal energy transport, radiation energy transport, ionization – affect the motion, and in the simulation code are added as source terms to the basic hydrodynamic equations.

We begin by considering motion in one dimension only. We also start with the simplest case of plasma that is a non-viscous and non-conducting fluid. Of course, real plasmas are both viscous and conducting, and we will learn how to add these descriptions to our mathematical modeling in later chapters. We are concerned with describing the bulk motion of the fluid rather than the thermal motion of the constituent particles, so a continuum fluid description will be adequate. We also assume that the bulk material velocities are much less than the velocity of light, so we can treat the fluid as non-relativistic.

Let us imagine that the plasma is confined inside a long cylinder whose axis is oriented along the $x$-coordinate direction, as illustrated schematically in Figure 4.1. We also imagine an infinitesimally narrow window of width $\delta x$ in the side of the cylinder at some position along its length that allows us to see and measure the plasma that is flowing past. What we see when looking in this window is mass flowing by, as well as momentum and energy.

The flux of any of these quantities is the product of the quantity's velocity $u$ and its density. Thus,

$$\text{flux of mass} = u\rho, \tag{4.1}$$

$$\text{flux of momentum} = u^2\rho, \tag{4.2}$$

$$\text{flux of energy} = u\rho\varepsilon, \tag{4.3}$$



https://doi.org/10.1017/CBO9781139095150.004 Published online by Cambridge University Press

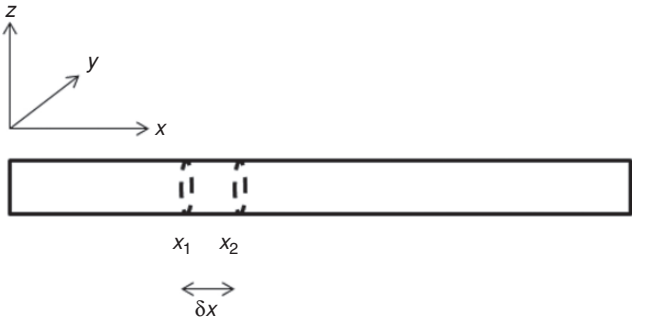


Figure 4.1 Schematic of plasma in a one-dimensional infinitely long cylinder flowing from left to right past a window of width $\delta x = x_2 - x_1$ in the side of the cylinder.

where $\rho$ is the mass density, $\varepsilon$ is the energy per unit mass (specific energy), and the momentum density is $\rho u$. Here we use the symbol $u$ to denote material flow velocity as distinct from particle velocities, which we denote with the symbol $v$.

Another way to understand the motion from the viewpoint of flux is to consider the amount of the given quantity that flows through the cross-sectional area $A$ of the cylinder past the window. It takes a time $\delta t = \delta x/u$ to flow past the window. Then, the volume of plasma flowing past the window in this time is $Au\delta t$. Since $\rho$ is the mass per unit volume, the total mass that flows by is $M = \rho Au\delta t$. Now, since the flux of mass is defined as the amount of mass passing through the cross-sectional area per unit of time, we find

$$\text{flux of mass} = M/A\delta t = u\rho. \tag{4.4}$$

Equation (4.4) is identical to equation (4.1). Equations (4.2) and (4.3) can be derived in similar fashion.

The fluxes given by equations (4.1) through (4.3) are convective fluxes. They describe that part of the total flux that results directly from the motion of the plasma itself. The convective flux may change as the plasma moves from one spatial position to another. In addition to the convective fluxes we must also consider the forces acting on the plasma as it moves to derive the equations of motion.

### *4.1.2 Conservation relations*

Let us consider again the plasma flowing past the cylinder window of Figure 4.1. We label as $x_1$ the spatial position on the left-hand side of the window, and as $x_2$ the spatial position on the right-hand side of the window, with the plasma flowing to the right from position $x_1$ to position $x_2$. At time $t_1$ an amount of mass equal to

$\rho A \delta x$ is in the window, and at the later time $t_2 = t_1 + \delta t$, an amount of mass equal to $\rho' A \delta x$ is in the window. Thus, over the elapsed time $\delta t$, the amount of mass in the window changes by an amount that is equal to the difference between the mass entering the window at position $x_1$ at time $t_1$ and the amount leaving at position $x_2$ at time $t_2$. We express this statement mathematically as

$$\rho' A \delta x - \rho A \delta x = (\rho u)_1 A \delta t - (\rho u)_2 A \delta t. \tag{4.5}$$

Equation (4.5) can be rewritten as

$$\frac{\rho' - \rho}{\delta t} = -\frac{(\rho u)_2 - (\rho u)_1}{\delta x}. \tag{4.6}$$

As both $\delta t$ and $\delta x$ go to zero, equation (4.6) becomes the partial differential equation

$$\frac{\partial \rho}{\partial t} = -\frac{\partial (\rho u)}{\partial x}. \tag{4.7}$$

Equation (4.7) expresses the conservation of mass, and is one of the three conservation relations that comprise the Navier–Stokes hydrodynamic equations. This equation relates two dependent variables, $\rho$ and $u$, as functions of the independent variables $x$ and $t$. Note the form of equation (4.7). It says that the time rate of change of mass density is equal to the negative spatial gradient of the mass flux.

We can use a similar line of reasoning to derive the other two conservation relations. For the conservation of momentum, we not only have the gradient in the convective momentum flux, but we have to account for the change in the momentum resulting from the force exerted on the plasma. From Newton's second law, this force is simply the spatial gradient of the pressure $P$. Thus, in analogy with the conservation of mass equation, equation (4.7), we can write the conservation of momentum equation as follows:

$$\frac{\partial (\rho u)}{\partial t} = -\frac{\partial \left(\rho u^2\right)}{\partial x} - \frac{\partial P}{\partial x}. \tag{4.8}$$

Note that the momentum conservation equation, equation (4.8), now adds another dependent variable, pressure $P$.

Again, in analogy to equations (4.7) and (4.8), we can write the energy conservation equation by equating the time rate of change of the energy density to the spatial gradient of the convective energy flux plus an additional term expressing the work done per unit time by the forces acting on the plasma. The work done is simply the product of the force and velocity. Thus, the energy conservation equation is

$$\frac{\partial (\rho \varepsilon)}{\partial t} = -\frac{\partial (\rho u \varepsilon)}{\partial x} - \frac{\partial (P u)}{\partial x}. \tag{4.9}$$

The energy conservation equation, equation (4.9), now adds yet another dependent variable, the total specific energy $\varepsilon$. We now have three equations of motion for the plasma – the three conservation equations that comprise the Navier–Stokes equations: conservation of mass, equation (4.7); conservation of momentum, equation (4.8); and conservation of energy, equation (4.9). These three equations comprise a set of coupled non-linear partial differential equations in four unknowns: density $\rho$, pressure $P$, velocity $u$, and specific energy $\varepsilon$. Thus, we need a fourth equation that does not introduce another dependent variable in order to solve this set of equations. The fourth equation is the equation of state (EOS), which we discuss in more detail in Chapter 6. As we shall see there, the EOS is derived from the thermodynamic relations. It relates pressure, density, and specific energy – thus, it does not introduce any new dependent variables – and is specific to the material and its phase.

The conservation relations can easily be generalized to three dimensions by replacing the partial derivative with respect to $x$ with the gradient operator, and writing the vector quantities in vector notation. Thus, we can rewrite equations (4.7), (4.8), and (4.9) as follows:

$$\frac{\partial \rho}{\partial t} + \nabla \cdot (\rho \mathbf{u}) = 0, \tag{4.10}$$

$$\frac{\partial (\rho \mathbf{u})}{\partial t} + \nabla \cdot (\rho \mathbf{u}\mathbf{u}) + \nabla P = 0, \tag{4.11}$$

$$\frac{\partial (\rho \varepsilon)}{\partial t} + \nabla \cdot (\rho \mathbf{u} \varepsilon) + \nabla (P \mathbf{u}) = 0. \tag{4.12}$$

This derivation of the Navier–Stokes equations is based on a continuum fluid picture of flux; that is, we have envisioned the plasma or fluid as a continuous medium in which the pressure, density, energy, and velocity vary smoothly or continuously in space.

The continuum fluid picture is fully consistent with the statistical picture of kinetic theory presented in Chapter 2. We can equivalently describe the plasma or fluid as a collection of point particles, as we did in Chapter 2. Indeed, we can also derive the Navier–Stokes equations – equations (4.10), (4.11), and (4.12) – from the Boltzmann equation, equation (2.11). We leave it as an exercise for the student to show how this is done.

Since plasma is composed of electrons and ions, the response of the lighter electrons to the pressure gradient terms will be different from that of the heavier ions. For example, the electric and magnetic fields act differently for the two species. In addition, we must add a term to the momentum conservation equation, equation (4.11), a coupling term $\mathbf{P}_{12}$ which accounts for collisions between the two species; the coupling term affects each particle species differently. At very

low density and/or high temperature the coupling becomes small and the electrons act independently of the ions, but the electric and magnetic fields still have major effects. The electrons move faster than the ions, and thus transport energy better, while the heavier ions transport the momentum. Therefore, we arrive at the conclusion that separate conservation equations are needed for the electron fluid and the ion fluid, but these separate equations are not independent of each other.

Note that both the conservation of mass equation [equation (4.10)] and the conservation of momentum equation [equation (4.11)] contain a term that describes the divergence of the velocity, $\nabla \cdot \mathbf{u}$. This term is just the dot product of the gradient operator with the velocity vector. In three-dimensional Cartesian coordinates, we can write this term as

$$\nabla \cdot \mathbf{u} = \frac{\partial u_x}{\partial x} + \frac{\partial u_y}{\partial y} + \frac{\partial u_z}{\partial z}. \tag{4.13}$$

For incompressible flow, in which $\partial\rho/\partial t = 0$, the divergence of the velocity, from equation (4.10), is identically equal to zero. Physically, this means that individual elements of the fluid do not spread out or bunch up anywhere. As an example, let us consider incompressible flow in two dimensions, $x$ and $y$. If we introduce another variable, a stream function $\psi$ that we define in such a way that

$$u_x = \frac{\partial \psi}{\partial y} \quad \text{and} \quad u_y = -\frac{\partial \psi}{\partial x}, \tag{4.14}$$

it is easy to see that for incompressible flow the function $\psi$ is constant along any line that is parallel to the velocity vector. These lines of constant $\psi$ are called streamlines of the flow.

For any incompressible flow that is also irrotational – that is, flow in which the vorticity, which is the curl of the velocity vector, is zero – the flow velocity can be written as the gradient of a velocity potential $\Psi$

$$\mathbf{u} = -\nabla\Psi. \tag{4.15}$$

Thus, the conservation of mass equation, equation (4.10), becomes identical to Poisson's equation, $\nabla^2\Psi = 0$. Analytic solutions can often be constructed for Poisson's equation.

In general, we will be challenged to describe flows that are neither incompressible nor irrotational, so the equations of motion cannot be solved analytically. In the more general case where the flow velocity varies in all three orthogonal coordinate directions – that is, each component of the velocity has a gradient in each of

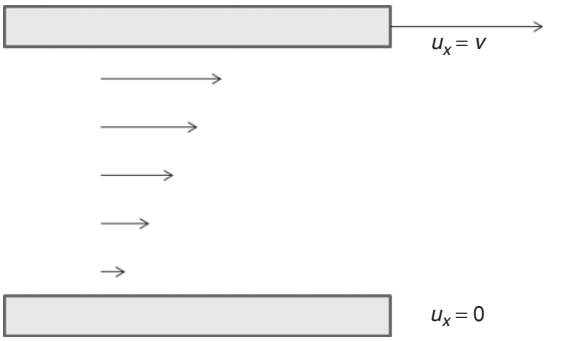


Figure 4.2 Illustration of planar Couette (shear) flow between an upper plate moving at velocity $v$ and a stationary lower plate.

the three coordinate directions – then the individual components of the velocity gradient become the elements of a three-by-three tensor:

$$\nabla \mathbf{u} = \begin{vmatrix} \dfrac{\partial u_x}{\partial x} & \dfrac{\partial u_y}{\partial x} & \dfrac{\partial u_z}{\partial x} \\ \dfrac{\partial u_x}{\partial y} & \dfrac{\partial u_y}{\partial y} & \dfrac{\partial u_z}{\partial y} \\ \dfrac{\partial u_x}{\partial z} & \dfrac{\partial u_y}{\partial z} & \dfrac{\partial u_z}{\partial z} \end{vmatrix} . \tag{4.16}$$

In this more general case, not only the velocity gradient becomes a tensor, but so does the pressure gradient. The equations of motion are then written in tensor form.

The tensor formulation is required to describe shear flows. In shear flows, one layer of the fluid may have a velocity component in, say, the $x$-direction, while in a direction orthogonal to this layer a neighboring layer will have a different $x$-component of velocity. One simple example of shear flow is planar Couette flow, as illustrated in Figure 4.2. Planar Couette flow occurs in a fluid or plasma contained between two parallel plates. In our example, the bottom plate is stationary, while the top plate has a velocity $v$ in the positive $x$-direction, as illustrated in Figure 4.2. The fluid in immediate contact with the plates has the same velocity as the plates. Thus, the fluid in the top layer has only an $x$-component of velocity, $u_x = v$, and the fluid in the bottom layer has a velocity $u_x = 0$. The velocities of the intermediate layers also have only an $x$-component of velocity, and this velocity component increases linearly from bottom to top. Thus, the only component of the velocity gradient we need to consider in solving the equations of motion for planar Couette flow is $\partial u_x / \partial y$.

### 4.1.3 Lagrangian derivative

The derivation of the conservation relations in the last section was based on a picture, as illustrated schematically in Figure 4.1, of an observer remaining at a fixed position in space and watching the plasma flowing past. We developed a mathematical description of the plasma properties based on this geometrical formulation. This formulation is called the Eulerian formulation.

Alternately, we can write the equations of motion in a formulation based on a picture in which the observer, instead of remaining at a fixed point in space, rides along with a mass element of the flowing plasma. In what is called the Lagrangian formulation, the equations of motion are expressions for the rate of change of the plasma properties along the motion of the plasma.

Let us start back at our original one-dimensional equations of motion, equations (4.7), (4.8), and (4.9). First we expand the partial derivatives. For example, the conservation of mass equation, equation (4.7), can be written

$$\frac{\partial \rho}{\partial t} + u\frac{\partial \rho}{\partial x} + \rho\frac{\partial u}{\partial x} = 0. \tag{4.17}$$

Likewise, the momentum conservation equation, equation (4.8), can be written

$$\rho\frac{\partial u}{\partial t} + u\frac{\partial \rho}{\partial t} + \rho u\frac{\partial u}{\partial x} + u\frac{\partial \rho u}{\partial x} + \frac{\partial P}{\partial x} = 0. \tag{4.18}$$

Now, multiply equation (4.17) by $u$, subtract the result from equation (4.18), and then divide each term by $\rho$. The result is

$$\frac{\partial u}{\partial t} + u\frac{\partial u}{\partial x} + \frac{1}{\rho}\frac{\partial P}{\partial x} = 0. \tag{4.19}$$

Similarly, the energy conservation equation, equation (4.9), can be written

$$\rho\frac{\partial \varepsilon}{\partial t} + \varepsilon\frac{\partial \rho}{\partial t} + \rho u\frac{\partial \varepsilon}{\partial x} + \varepsilon\frac{\partial \rho u}{\partial x} + \frac{\partial P u}{\partial x} = 0. \tag{4.20}$$

Now, multiply equation (4.17) by $\varepsilon$, subtract the result from equation (4.20), and then divide each term by $\rho$. The result is

$$\frac{\partial \varepsilon}{\partial t} + u\frac{\partial \varepsilon}{\partial x} + \frac{1}{\rho}\frac{\partial P u}{\partial x} = 0. \tag{4.21}$$

Equations (4.17), (4.19), and (4.21) are the new equations of motion. Note that the first two terms of each of these three equations have the same form. The first term is the Eulerian time derivative. The second term is the advection term, describing

how the dependent variable changes as it moves. Note that these two terms together can be rewritten as a single Lagrangian time derivative,

$$\frac{d}{dt} = \frac{\partial}{\partial t} + \frac{\partial}{\partial x}\left(\frac{dx}{dt}\right), \tag{4.22}$$

converting the PDEs into ordinary differential equations (ODEs). In the 1D case we are considering here, however, $dx/dt = u$, the fluid velocity. Thus, we can now rewrite the three equations of motion in Lagrangian formulation as

$$\frac{d\rho}{dt} + \rho\frac{\partial u}{\partial x} = 0, \tag{4.23}$$

$$\frac{du}{dt} + \frac{1}{\rho}\frac{\partial P}{\partial x} = 0, \tag{4.24}$$

$$\frac{d\varepsilon}{dt} + \frac{1}{\rho}\frac{\partial (Pu)}{\partial x} = 0. \tag{4.25}$$

The equations of motion – the Navier–Stokes equations – form the foundation of any physical description of the properties and behavior of matter at extreme conditions. In the Eulerian formulation [equations (4.7), (4.8), and (4.9) in 1D, equations (4.10), (4.11), and (4.12) in 3D] the fluid element size, or volume, remains constant, and the mass density of the fluid or plasma contained in the fluid element varies because the mass flowing through the element changes with time. In contrast, in the Lagrangian formulation [equations (4.23), (4.24), and (4.25) in 1D] the fluid element mass remains constant, and the mass density of the fluid or plasma contained in the fluid element varies because the volume of the fluid element changes with time. These two descriptions are mathematically equivalent. The two formulations yield the same solution for the dependent variables as a function of spatial position and time. As we discuss in more detail in Chapter 11, however, for some classes of problems it is more advantageous to use an Eulerian formulation, and for other classes of problems it is more advantageous to use a Lagrangian formulation. There are also a number of hybrid formulations that can facilitate obtaining numerical solutions of the equations of motion.

Before we get to discussing numerical solutions of the equations of motion, we need to discuss some properties and physical consequences of these equations.

### *4.1.4 Scaling and self-similarity*

We cannot create plasmas in the laboratory on the same spatial and time scales as astrophysical plasmas – galactic jets, for example – but we can create plasmas for which the flow variables of the astrophysical plasma can be derived by simply changing the basic scales of length, time, and/or density.

https://doi.org/10.1017/CBO9781139095150.004 Published online by Cambridge University Press

This is possible because the equations of motion are invariant under certain scaling transformations. Recall that the equations of motion express three dependent variables – $\rho$, $P$, and $u$ – as functions of spatial position, $\mathbf{r}$, and time, $t$. This statement is written mathematically as $\rho = \rho(\mathbf{r}, t)$, $P = P(\mathbf{r}, t)$, and $u = u(\mathbf{r}, t)$. The specific energy $\varepsilon$ can be written, via the equation of state, in terms of pressure and density, so it is not independent of the other dependent variables. It is sufficient, therefore, to look only at how transformations of the pressure, density, and velocity alter the equations of motion.

First note that the independent variables $\mathbf{r}$ and $t$ enter the 1D equations of motion only in the derivatives. Thus, any linear shift in these variables leaves the 1D equations unchanged. For example, a shift in time, achieved by replacing the variable $t$ by a new variable $t' = t + t_0$, does not alter the equations of motion. Similarly, a shift in spatial position, achieved by replacing the variable $x$ by a new variable $x' = x + x_0$ – corresponding to selecting a new origin for the coordinate system – also does not alter the 1D equations of motion. The 1D equations are said to be invariant under linear transformations of the independent variables. In cylindrical or spherical geometry, however, the equations are not invariant under linear transformation of the spatial variable. We leave proof of this statement as an exercise for the student.

The dimensions of velocity are length divided by time. Thus, the equations of motion are invariant under any scale transformation that multiplies the length and time scales by the same constant scale factor, while leaving the density and pressure scales unchanged. This transformation is achieved by replacing the variable $x$ by a new variable $x' = s_x x$ and simultaneously replacing the variable $t$ by a new variable $t' = s_x t$, where $s_x$ is some constant scale factor. The new motion is similar to the old one, differing only in the length and time scales.

The dimensions of pressure are density multiplied by length squared and divided by time squared. Thus, the equations of motion are invariant under any scale transformation that multiplies the pressure and density scales by the same constant scale factor. This transformation is achieved by replacing the variable $P$ by a new variable $P' = s_P P$ and simultaneously replacing the variable $\rho$ by a new variable $\rho' = s_P \rho$, where $s_P$ is some constant scale factor. The new motion is similar to the old one, differing only in the pressure and density scales.

It is easy to see that the equations of motion are invariant under both transformations simultaneously. This is true whether $s_x = s_P$ or $s_x \neq s_P$. Pressure and density, however, are not independent of one another. They are related via the equation of state. Thus, the equation of state must allow the $s_P$ scale transformation. A perfect gas equation of state, for which pressure is directly proportional to density, allows such a scale transformation. A general equation of state, however, does not, but it may allow an invariant transformation for a scale factor $s_t$ applied to a time variable

different from the scale factor $s_x$ applied to the spatial variable, and with the three scale factors related in some way. For example, it can be shown that the equations of motion for electron plasma described by a Fermi–Dirac equation of state are invariant under scale transformations for which

$$s_x = s_t s_P^{1/3}. \tag{4.26}$$

Motion under these scale transformations is said to be self-similar. Using these transformations it is possible to create plasmas in the laboratory that are similar in their hydrodynamic properties to plasmas that cannot be replicated in the laboratory. This is possible, however, only when other physical processes that affect the pressure, density, and velocity are absent or negligible, such as viscosity and radiation energy transport. Plasmas in which these other processes play a large role are not self-similar under scale transformations.

## 4.2 Compression and rarefaction waves

### *4.2.1 Acoustic waves, sound speed*

Consider once again a 1D plasma in which the spatial and temporal variations in density and pressure are small with respect to the average or at-rest density $\rho_0$ and pressure $P_0$; that is,

$$\rho = \rho_0 + \Delta\rho, \tag{4.27}$$

$$P = P_0 + \Delta P. \tag{4.28}$$

Now substitute equations (4.27) and (4.28) into the conservation of mass equation [equation (4.23)] and the conservation of momentum equation [equation (4.24)]. Since $\Delta\rho \ll \rho_0$ and $\Delta P \ll P_0$ we can ignore the terms in the gradients containing $\Delta\rho$ and $\Delta P$. The result is as follows:

$$\frac{d(\Delta\rho)}{dt} = -\rho_0 \frac{\partial u}{\partial x}, \tag{4.29}$$

$$\rho_0 \frac{du}{dt} = -\frac{\partial P}{\partial x}. \tag{4.30}$$

Equation (4.30) can be rewritten as

$$\rho_0 \frac{du}{dt} = -\left(\frac{\partial P}{\partial \rho}\right) \frac{\partial (\Delta\rho)}{\partial x}. \tag{4.31}$$

https://doi.org/10.1017/CBO9781139095150.004 Published online by Cambridge University Press

Now, differentiate equation (4.29) with respect to $t$ and differentiate equation (4.31) with respect to $x$. We then find

$$\frac{\partial^2(\Delta\rho)}{\partial t^2} = c_s^2 \frac{\partial^2(\Delta\rho)}{\partial x^2}, \tag{4.32}$$

where

$$c_s^2 = \left(\frac{\partial P}{\partial \rho}\right). \tag{4.33}$$

Equation (4.32) is the classical wave equation, which has the solution

$$\Delta\rho = \exp\{i\,(x \pm c_s t)\}\,. \tag{4.34}$$

Thus, the equations of motion for small perturbations lead directly to the wave equation. The wave equation says that small variations in density and pressure propagate in both directions in the plasma at velocity $c_s$, which is called the adiabatic sound speed. The sound speed, from equation (4.33), is a function of the material's equation of state, which relates the material's pressure to its density and specific energy.

Note that the square of the adiabatic sound speed is inversely proportional to the material's compressibility. Typically, a gas is much more compressible than a solid; that is, much less pressure is required to compress a gas by a certain fractional amount than the pressure required to compress a solid by the same fractional amount. Thus, the sound speed in solids is typically much greater than the sound speed in gases. The adiabatic sound speed for a few select materials is given in Appendix III.

### *4.2.2 Characteristics of the flow*

Now we examine properties of the Navier–Stokes equations that allow us to elucidate characteristics of the hydrodynamic motion. Consider any disturbance created in a 1D fluid at time $t_0$ originating at position $x_0$. These disturbances will propagate in both directions at the sound speed, $c_s$. Since the flow is assumed isentropic,

$$\Delta P = c_s^2 \Delta\rho, \tag{4.35}$$

and the velocities in each disturbance are

$$u = \pm\frac{\Delta P}{\rho_0 c_s} = \pm\frac{c_s}{\rho_0}\Delta\rho. \tag{4.36}$$

For small disturbances in the flow, that is, $\Delta\rho \ll \rho_0$, the flow or particle velocity is much less than the acoustic wave velocity. The disturbances themselves travel in both directions from some initial point $x_0$ at time $t_0$ at velocity $u_0 \pm c_{s0}$. Since

$u$ and $c_s$, in general, vary from point to point in the flow from their initial values $u_0$ and $c_{s0}$ at $x_0$ and $t_0$, the paths in the $(x, t)$ plane along which the disturbances propagate trace out curves in the plane, that is,

$$\frac{dx}{dt} = u \pm c_s. \tag{4.37}$$

These curves are called the characteristic curves of the flow. We now derive expressions for these characteristic curves using the conservation relations.

First, we rewrite the conservation of momentum equation in Eulerian form, equation (4.19), after substituting in equation (4.33), the definition of the acoustic wave velocity:

$$\rho\left(\frac{\partial u}{\partial t} + u\frac{\partial u}{\partial x}\right) + c_s^2\frac{\partial \rho}{\partial x} = 0. \tag{4.38}$$

Now, multiply the conservation of mass equation in Eulerian form, equation (4.17), by $c_s^2/\rho$, divide equation (4.38) by $\rho$, and then add the two resulting equations. The result is:

$$\frac{c_s}{\rho}\frac{\partial \rho}{\partial t} + \frac{c_s}{\rho}u\frac{\partial \rho}{\partial x} + c_s\frac{\partial u}{\partial x} + \frac{\partial u}{\partial t} + u\frac{\partial u}{\partial x} + \frac{c_s^2}{\rho}\frac{\partial \rho}{\partial x} = 0. \tag{4.39}$$

Define a new variable

$$\omega(x, t) = \int c_s\frac{\partial \rho}{\rho}, \tag{4.40}$$

which has units of velocity, and is essentially a density-weighted average adiabatic sound speed.

Thus,

$$\frac{\partial \omega}{\partial t} = \frac{c_s}{\rho}\frac{\partial \rho}{\partial t} \quad \text{and} \quad \frac{\partial \omega}{\partial x} = \frac{c_s}{\rho}\frac{\partial \rho}{\partial x}. \tag{4.41}$$

Then, using equations (4.41), equation (4.39) becomes

$$\frac{\partial \omega}{\partial t} + \frac{\partial u}{\partial t} + (u + c_s)\left(\frac{\partial \omega}{\partial x} + \frac{\partial u}{\partial x}\right) = 0. \tag{4.42}$$

Now, we define $r = (\omega + u)/2$, so equation (4.42) becomes

$$\frac{\partial r}{\partial t} + (u + c_s)\frac{\partial r}{\partial x} = 0. \tag{4.43}$$

Equation (4.43) says that lines of constant $r$ are propagated with velocity $u + c_s$ in the $(x, t)$ plane. That is, if $r(x, t)$ is a solution of equation (4.43), then $r[x + (u + c_s)t, t]$ is also a solution. The line of slope $(u + c_s)$ in the $(x, t)$ plane is called the characteristic line.

https://doi.org/10.1017/CBO9781139095150.004 Published online by Cambridge University Press

Similarly, if we define $s = (u - \omega)/2$, we can derive an equation similar to equation (4.43):

$$\frac{\partial s}{\partial t} + (u - c_s)\frac{\partial s}{\partial x} = 0. \tag{4.44}$$

Here, lines of constant $s$ are propagated with velocity $u - c_s$ in the $(x, t)$ plane. These lines are called the cross-characteristics.

Determining the characteristics of the flow by solving equations (4.43) and (4.44) can be, in some special cases, a particularly effective way to visualize the hydrodynamic behavior. In Section 4.2.4 we apply the method of characteristics to the special case of the adiabatic expansion of a perfect gas.

### *4.2.3 Compression waves and shock fronts*

Let us return to the picture of Figure 4.1, but instead of considering plasma flowing through a section of pipe of infinite length, as illustrated in Figure 4.1, let us imagine that, at the left boundary there is a piston and that at time zero there is no plasma to the left of the piston, and the plasma in the pipe to the right of the piston is at rest.

Now, at time $t_0$ let us move the piston to the right, into the plasma, compressing it. A compression wave moves to the right into the plasma at the acoustic wave velocity (sound speed) of the at-rest plasma, $c_{s0}$. At the same time, the particles of the plasma at and near the piston are set into motion at the velocity of the piston, $u_p$. The piston does work on the plasma, so not only does the plasma kinetic energy increase as the plasma is compressed by the piston, but so does the plasma internal energy. Thus, in general, the sound speed in the plasma near the moving piston increases. Thus, at some time $t > t_0$, the piston is at the position $x_p = x_0 + u_p t$ and the compression wave front is at the position $x_s = x_0 + c_{s0}t$, with $x_s > x_p$. There are now two regions in the plasma, as illustrated in Figure 4.3. The plasma to the right of the compression wave remains at rest, uncompressed and undisturbed. The plasma located between the piston and the compression wave is moving to the right at velocity $u_p$ and has density, pressure, and specific energy greater than those in the undisturbed plasma.

Let us now consider that the piston velocity increases with time. Let us approximate the piston acceleration by a sequence of small velocity jumps at closely spaced time intervals. Each jump in velocity of the piston launches a new compression wave into the plasma, at an adiabatic compression wave velocity faster than the one launched at the previous time interval. Given enough time and run distance in the plasma, the later compression waves can catch up to the earlier ones. The result is a "piling up" of these compression waves, along with a narrowing of the region over which the flow variables transition from the undisturbed state ahead of the

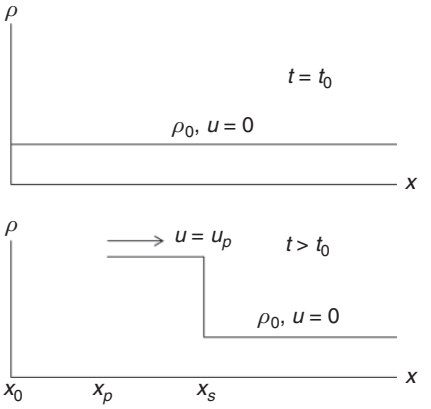


Figure 4.3 Density profiles at time zero, $t_0$, and at some later time $t > t_0$ in a one-dimensional plasma compressed from the left by a constant-velocity piston.

wave and the compressed state behind the wave. A shock wave is formed by this piling up of compression waves in a narrow wave front.

Formation of a shock wave is not unlike the formation of breakers at the sea shore. Waves on the open ocean travel at the adiabatic sound speed. As these waves approach the shore they propagate into shallower water. As the troughs of the wave begin to contact the ocean bottom, frictional drag causes the wave speed to decrease. Thus, the waves in the deeper water behind begin to pile up onto the slower waves in front. As more and more waves pile up, the wave front steepens. Once the wave front is steep enough it crashes over itself into a breaker. Here the analogy to shock formation in plasma breaks down, because in a gas or plasma the steepened wave front propagates as a shock wave and does not crash over itself as a breaker.

The physics of shocks is treated in more detail in the next chapter. There we will use the conservation equations to derive the Rankine–Hugoniot equations that relate the equilibrium conditions in front of the shock to the equilibrium conditions behind the shock; consider the behavior of shocks at boundaries and interfaces; introduce the concepts of entropy and viscosity in describing the structure and thickness of the shock wave front; and discuss the physics of the special cases of shock waves in a highly compressible gas, like air, and shock waves in solids. Before we get to our more detailed discussion of shock waves, though, we first discuss rarefaction waves and hydrodynamic instabilities.

### *4.2.4 Rarefaction waves and rarefaction shocks*

Now let us go back to our picture of the piston at the left boundary of the 1D pipe. This time, however, we will move the piston to the left. As the piston moves, the

https://doi.org/10.1017/CBO9781139095150.004 Published online by Cambridge University Press

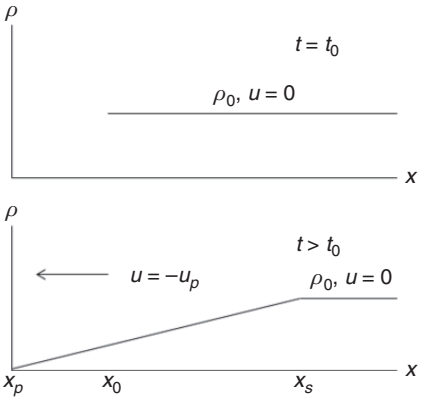


Figure 4.4 Density profiles at time zero, $t_0$, and at some later time $t > t_0$ in a one-dimensional plasma expanded to the left as a constant-velocity piston is withdrawn.

plasma does work on it as it expands into the space opened up between the at-rest plasma and the moving piston, giving up some of its internal energy to kinetic energy. Thus, the adiabatic sound speed in the expanding plasma near the piston is less than in the plasma at rest. At some time $t > t_0$, the piston is at the position $x_p = x_0 - u_p t$ and there is some region of expanded plasma between $x_p$ and the region of undisturbed plasma in which the pressure, density, and adiabatic sound speed are less than they are in the undisturbed plasma, as illustrated in Figure 4.4. While the piston moves to the left, the initial disturbance at $x_0$ and $t_0$ propagates to the right as a rarefaction wave at the sound speed in the undisturbed plasma. Thus, the boundary between the rarefied and the undisturbed plasma at time $t$ is $x_s = x_0 + c_{s0}t$, as shown in Figure 4.4.

Both compression waves and rarefaction waves travel into the undisturbed plasma at the adiabatic sound speed. There is, however, a fundamental difference between the two types of waves. Compression waves, as we have seen, can pile up into a shock, because, in general, the sound speed in the compressed plasma is greater than the sound speed in the uncompressed plasma. A rarefaction wave, though, cannot, in general, steepen into a shock. Any perturbation in the velocity of the withdrawing piston, whether an acceleration or deceleration, will launch a disturbance in the expanding plasma that will be propagated at a sound speed less than the sound speed at which the rarefaction wave is traveling into the undisturbed plasma. These later disturbances, then, cannot catch up to the original disturbance.

There is, however, a circumstance in which rarefaction shocks can form. If the expanding plasma undergoes a phase transition upon expansion to a lower density in which the sound speed in the material in its new phase is greater than the sound

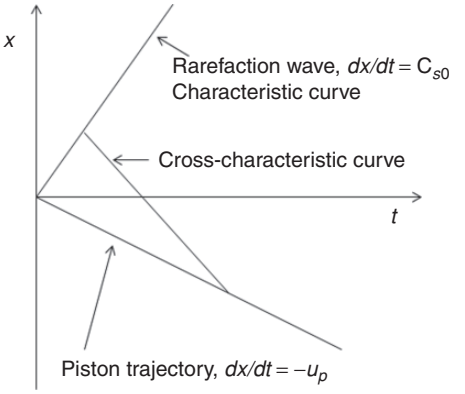


Figure 4.5 Characteristic curves for a rarefaction wave.

speed in the original phase, then it is possible for a shock to form in the rarefying material. We will say more about rarefaction shocks in Chapter 6.

Finally, we look at the characteristic solutions for a rarefaction wave traveling into plasma that is initially at rest. Let us again assume that the piston is at position $x_0$ at time $t_0$, and then moves to the left at constant velocity $u_p$. The characteristic line defined by $dx/dt = u + c_s$, equation (4.37), becomes $dx/dt = c_{s0}$, since the flow velocity $u = 0$ everywhere to the right of the rarefaction wave front, and the sound speed here is the sound speed in the undisturbed plasma, $c_{s0}$. Thus, the characteristic line is coincident with the trajectory in the $(x, t)$ plane of the rarefaction wave, as shown in Figure 4.5. The trajectory of the piston is also shown in Figure 4.5.

The cross-characteristic line defined by $dx/dt = u - c_s$ has negative slope between the rarefaction wave trajectory and the piston trajectory, because in this region $u < 0$ (the plasma is expanding to the left) and $c_s \geq 0$. In addition, the slope is more negative than that of the piston trajectory, assuming $c_s \neq 0$ anywhere within the flow in this region, so each cross-characteristic line, as also shown in Figure 4.5, intersects the piston trajectory as well as crossing the characteristic line. Thus, from equation (4.44), we can write

$$u_0 - \omega_0 = u_p - \omega_p \tag{4.45}$$

[the variables $\omega$ are defined in equation (4.40)] or, since $u_0 = 0$,

$$\omega_p = u_p + \omega_0. \tag{4.46}$$

For a polytropic perfect gas, for example,

$$\omega = \frac{2c_s}{\gamma - 1}, \tag{4.47}$$

https://doi.org/10.1017/CBO9781139095150.004 Published online by Cambridge University Press

where $\gamma$, the adiabatic index, is the constant ratio of specific heats. We define and discuss specific heat and the adiabatic index in the next chapter. Thus, equation (4.46) becomes

$$c_{sp} = \frac{\gamma - 1}{2} u_p + c_{s0}. \tag{4.48}$$

Here, $c_{sp}$ is the sound speed in the plasma at the piston. Since $u_p < 0$, then $c_{sp} < c_{s0}$. The more negative the piston speed – that is, the faster it is withdrawn to the left – the smaller the sound speed at the piston. If the piston is withdrawn at a velocity faster than the critical velocity at which $c_{sp} = 0$, then the plasma cannot follow, and a vacuum region opens up between the expanding plasma and the piston. This critical velocity is called the escape velocity of the plasma. For a polytropic perfect gas, the escape velocity is

$$u_{\text{escape}} = -\frac{2c_{s0}}{\gamma - 1}. \tag{4.49}$$

The escape velocity is independent of time because the adiabatic sound speed in the undisturbed plasma is independent of time. We will return to this question of the escape velocity when we consider the emergence of shocks at a free surface in the next chapter.

## 4.3 Hydrodynamic instabilities

Up to now, we have focused our discussion mainly on one-dimensional motion. The one-dimensional description is adequate for illustrating the principal features and characteristics of hydrodynamic motions, and for deriving the basic equations of motion, as we did earlier in this chapter. With a one-dimensional description we were able to elucidate the main features of acoustic waves, compression waves, rarefaction waves, shocks, and self-similarity. We were also able easily to generalize the equations to three dimensions.

There are some important features of hydrodynamic motion, however, that cannot be described in one dimension. Vortex flow, for example, is intrinsically multi-dimensional, since one must calculate the curl of the velocity vector to describe vortex motion. Another important example is the unstable growth of perturbations in the flow. Hydrodynamic instability growth is intrinsically multi-dimensional. We now turn our attention to a discussion of hydrodynamic instabilities, a phenomenon of great importance in many extreme physics environments, including supernovae explosions and inertial fusion capsule implosions.

### 4.3.1 Rayleigh–Taylor instability

The Rayleigh–Taylor instability, which we will hereinafter refer to as the RT instability, occurs when a lower-density fluid or plasma accelerates a higher-density fluid or plasma. This instability causes a perturbation at the interface between the two plasmas to grow into spikes of the higher-density plasma penetrating into the lower-density plasma, while bubbles of the latter buoyantly rise into the denser plasma. Thus, any interface between two different materials at different densities can be unstable as the interface gets accelerated in the direction of the denser material. Indeed, in order to be unstable the interface does not necessarily have to separate two different materials; it could also be an interface between two different phases of the same material – a phase boundary, for example – or even a boundary that separates two regions of different density of the same material.

The RT instability is a common phenomenon throughout nature. It is responsible for water dripping from a kitchen faucet and for the mixing of heavier core material with lighter envelope material in a supernova explosion. In the case of the water drop hanging off the end of the faucet, the drop is initially in static equilibrium as the force of gravity is balanced by the adhesion forces holding the drop onto the inside surface of the faucet. The interface between the water drop and the air, however, is not flat; it forms into a curved surface as a result of surface tension, and thus does not follow a surface of constant gravitational potential. This perturbed interface is then RT unstable as the higher-pressure but lower-density air pushes on the lower-pressure but higher-density water. As a result, the perturbation of the interface – its curvature – grows with time, until the drop detaches from the faucet. Perturbed interfaces that separate different densities can be RT unstable whether the separate materials are incompressible – as in the dripping water example – or compressible – as in a supernova explosion. The only requirement for the instability is that the pressure gradient and the density gradient be in opposite directions at the interface.

Let us consider an interface between two regions of different densities on which there is a sinusoidal perturbation with wavelength $\lambda$, as illustrated in Figure 4.6. Let us assume that the denser material is on top, that is, $\rho_2 > \rho_1$, and that the interface is accelerated upward, as shown in Figure 4.6. We have oriented the coordinate system such that the unperturbed interface is entirely in the $(x, y)$ plane, and the growth of the perturbation is in the $z$-direction. We can thus write the material velocity as

$$u(x, y, z) = u_z \exp\left(ik_x x + ik_y y + \gamma t\right), \tag{4.50}$$

https://doi.org/10.1017/CBO9781139095150.004 Published online by Cambridge University Press

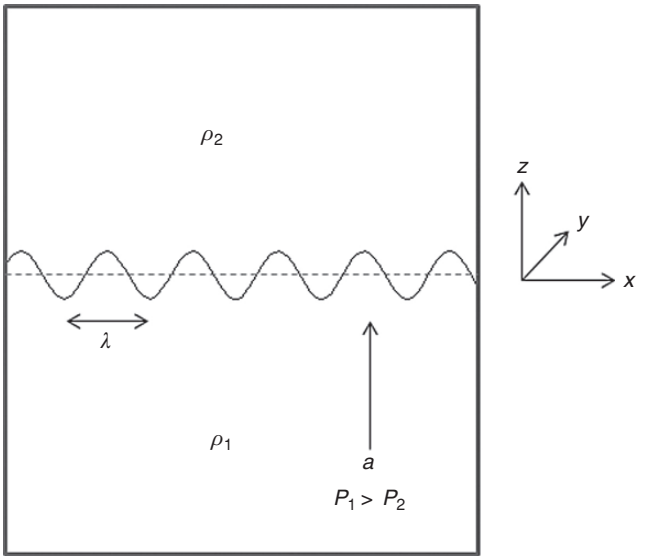


Figure 4.6 A sinusoidal perturbation with wavelength λ and amplitude $\eta$ on an interface between two uniform plasmas of different density. The unperturbed interface is shown by the dashed line.

where

$$k = \frac{2\pi}{\lambda} = \left(k_x^2 + k_y^2\right)^{1/2}. \tag{4.51}$$

In order to derive an expression for the growth rate $\gamma$ of this interface perturbation, let us start with the assumption that the amplitude $\eta$ of the perturbation is small, that is, $\eta \ll \lambda$, and hence the density and pressure variations in the perturbation are small, that is, $P = P_0 + \delta P$ and $\rho = \rho_0 + \delta\rho$. It is customary to use the symbol $\gamma$ for the perturbation growth rate, but it is not to be confused here with the adiabatic index (ratio of specific heats) used in equations (4.47), (4.48), and (4.49) above, which is denoted by the same symbol.

We can further assume that the interface perturbation, in this linear growth range, is incompressible, that is, $\nabla \cdot \mathbf{u} = 0$. Although the perturbation is assumed to be incompressible, the main body of the two plasmas does not necessarily have to be incompressible. With these assumptions, we can linearize the equations of motion. The mass conservation and momentum conservation equations, equations (4.10) and (4.11), in linearized form, and assuming incompressibility of the perturbation, become

$$\frac{\partial \delta\rho}{\partial t} + \mathbf{u} \cdot \nabla\rho = 0 \tag{4.52}$$

https://doi.org/10.1017/CBO9781139095150.004 Published online by Cambridge University Press

and

$$\rho \frac{\partial \mathbf{u}}{\partial t} = -\nabla \delta P - a \delta \rho \mathbf{z}, \tag{4.53}$$

where $a$ is the constant acceleration of the interface and $\mathbf{z}$ is a unit vector in the $z$-direction, the direction of the acceleration. Now, substituting equation (4.50) into equations (4.52) and (4.53) yields the following four equations for each of the velocity components:

$$\rho u_x \gamma = -ik_x \delta P, \tag{4.54}$$

$$\rho u_y \gamma = -ik_y \delta P, \tag{4.55}$$

$$\rho u_z \gamma = -\frac{\partial}{\partial z} \delta P - a \delta \rho, \tag{4.56}$$

$$\gamma \delta \rho = -u_z \frac{\partial \rho}{\partial z}. \tag{4.57}$$

Now, we multiply equation (4.54) by $-ik_x$, multiply equation (4.55) by $-ik_y$, add the two resulting equations, and simplify the result by making use of the vanishing of the divergence of the velocity, along with equation (4.51). The final result is

$$\rho \gamma \frac{\partial u_z}{\partial z} = -k^2 \delta P. \tag{4.58}$$

Next, substitute equation (4.57) into equation (4.56):

$$\rho u_z \gamma = -\frac{\partial}{\partial z} \delta P + u_z \frac{a}{\gamma} \frac{\partial \rho}{\partial z}. \tag{4.59}$$

Finally, solve equation (4.58) for $\delta P$ and substitute into equation (4.59), which yields the equation of motion for single-mode planar RT instability growth:

$$\frac{\partial}{\partial z} \left[ -\rho \gamma \frac{\partial u_z}{\partial z} \right] = k^2 \left[ -\rho u_z \gamma + u_z \frac{a}{\gamma} \frac{\partial \rho}{\partial z} \right]. \tag{4.60}$$

The boundary conditions on equation (4.60) are that both $u_z$ and $\partial u_z / \partial z$ must be continuous across the interface. Thus, we can write the boundary conditions as

$$u_0 \frac{a}{\gamma} (\rho_2 - \rho_1) = \frac{\gamma}{k} (\rho_2 + \rho_1) u_0, \tag{4.61}$$

where $u_0$ is the initial velocity of the interface. From equation (4.61) we obtain the growth rate

$$\gamma = \sqrt{Aka}, \tag{4.62}$$

https://doi.org/10.1017/CBO9781139095150.004 Published online by Cambridge University Press

where

$$A = \frac{\rho_2 - \rho_1}{\rho_2 + \rho_1} \tag{4.63}$$

is defined as the Atwood number. Note that, for unstable growth, $A$ can have values only between 0 and 1. When the densities on either side of the interface are the same, $A = 0$ and there is no growth of the perturbation since there is no interface between different-density regions. When $\rho_2 \gg \rho_1$, $A \approx 1$, and the growth rate assumes its maximum value for a given mode. That is, the larger the difference between the densities on either side of the interface, the faster the growth rate for a given mode. When $\rho_1 > \rho_2$, $A$ is negative, and then, according to equation (4.63), the perturbation does not grow exponentially with time, but instead oscillates around its initial amplitude. The initial perturbation grows only when the less-dense material accelerates the more-dense material.

### *4.3.2 Stabilization mechanisms*

The classical RT growth rate, given by equation (4.62), is the fastest rate at which an unstable interface perturbation can grow. A number of effects can reduce the classical RT growth rate, including surface tension, a density gradient, ablation, and viscosity. The RT instability can also occur at the surface of a solid that is accelerated by a lower-density fluid or plasma. In that case, the material strength of the solid plays a role in stabilizing or reducing the perturbation growth in the solid state. We will consider solid-state RT instabilities in Chapter 5. Here we will discuss briefly the other mechanisms by which RT growth can be reduced or even stabilized.

We will not, however, discuss surface tension, an effect that plays almost no role in the extreme physics environments in which we are concerned. The interested student may consult the fairly extensive journal literature on this topic, starting with the work of Bellman and Pennington in 1954, and moving on to the more recent work of Mikaelian. Both of these articles are listed in the Further Reading.

As we saw in the previous subsection, the RT growth rate depends on the square-root of the Atwood number. The larger the jump in density at the interface, the larger the growth rate. Thus, the growth rate may be reduced by essentially reducing the density gradient at the interface, or by "smearing out" the interface. It can be shown (but we will not do so here) that the single-mode RT growth rate with density-gradient stabilization can be well approximated by

$$\gamma_L = \sqrt{\frac{Aka}{1 + kL}}. \tag{4.64}$$

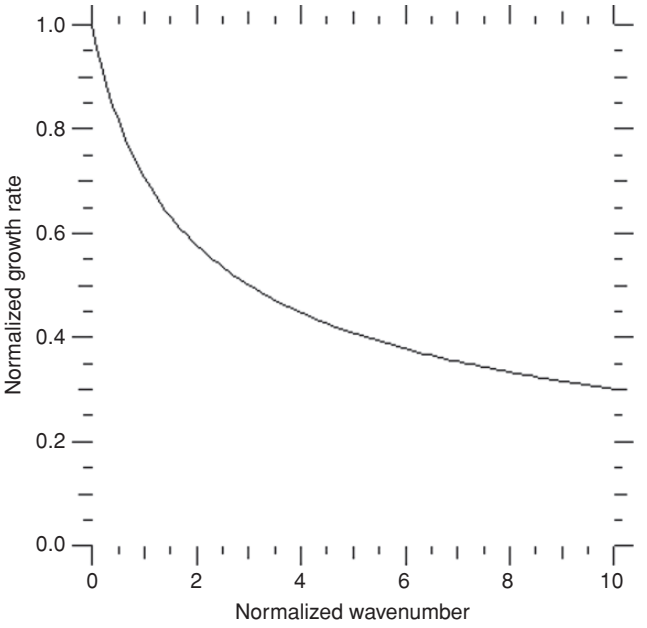


Figure 4.7 The normalized density-gradient-stabilized RT instability growth rate $\gamma_L/\gamma$ versus normalized wavenumber $kL$, with $L = \rho/\nabla\rho$.

Here, $L = \rho/\nabla\rho$ is the density-gradient scale length. Note that the larger the density-gradient scale length for a given mode, the more the growth rate is reduced. In other words, the more the interface is smeared out, the less the interface perturbation grows.

In addition, we see that if the wavelength of the perturbation is large compared to the density-gradient scale length (i.e., $kL \ll 1$), there is little reduction of the growth rate below its classical value. Wavelengths that are small compared to the density-gradient scale length, however, have much reduced growth. In such a situation the perturbation, in its linear growth phase, does not experience a large difference in density. In Figure 4.7 we plot the ratio of the density-gradient-stabilized growth rate $\gamma_L$ to the classical growth rate $\gamma$ as a function of the normalized wavenumber $kL$. We see that all modes grow in a density gradient at an unstable interface, but the large mode numbers (small wavelengths) grow so slowly that in a simulation of mode growth in such plasma we can ignore these modes. Thus, we can define an effective cutoff wavelength below which the RT growth is negligibly small. This cutoff wavelength, of course, depends on the evolving state characteristics of the plasma, and thus may change with time. It must be chosen carefully to capture accurately the particular behavior we wish to model.

In the laser ablation process that we considered in Chapter 3, the hot ablated plasma is at much higher pressure than the higher-density unablated material. Thus, the interface between these two regions is classically RT unstable. In fact, ablation-front RT instability growth has remained one of the primary obstacles to making high-gain laser-driven inertial fusion work. The RT-unstable perturbations at the ablation surface of an imploding ICF capsule can grow large enough to feed-through the shell, leading to break-up of the imploding shell and failure to compress the fusion fuel contained within the shell. In classical RT, the higher mode numbers grow faster. It is these higher-mode perturbations, though, that are preferentially "fire-polished" away by the ablation process itself. The ablation-stabilized RT growth rate is

$$\gamma_a = \sqrt{Aka} - \beta k v_a, \tag{4.65}$$

where $v_a$ is the ablation velocity and $\beta$ is a constant, which typically must be determined by measurement.

Note that the growth rate of all modes is reduced by ablation, with more reduction at larger mode numbers. Indeed, the growth rate is zero for all wavenumbers larger than a cutoff wavenumber

$$k_c = \frac{Aa}{(\beta v_a)^2}. \tag{4.66}$$

Thus, the normalized ablation-stabilized growth rate can be written

$$\frac{\gamma_a}{\gamma} = 1 - \sqrt{\frac{k}{k_c}}. \tag{4.67}$$

We plot equation (4.67) in Figure 4.8. Note that, because of ablation stabilization, all modes with wavelengths less than $\lambda_c = 2\pi/k_c$ are completely stabilized and do not grow. This is good news for inertial confinement fusion, because, in principle, we do not have to worry about polishing away the small-scale surface roughness on the outside surface of the shell. The ablation process itself does this polishing for us. Simulations of imploding shells have shown that the most unstable mode is typically the mode with a wavelength comparable to the shell thickness. Thus, for the outside surface of the imploding shell, mode numbers less than about one-sixth of the shell's in-flight aspect ratio are the most worrisome. The shell aspect ratio is the ratio of the shell radius to its thickness, which typically increases initially as the shell compresses. So, there is an advantage in imploding shells that are as round as we can make them, and not too thin. Thicker shells, of course, are more massive and hence require more drive energy. One must consider carefully all these tradeoffs in designing an optimum inertial fusion capsule.

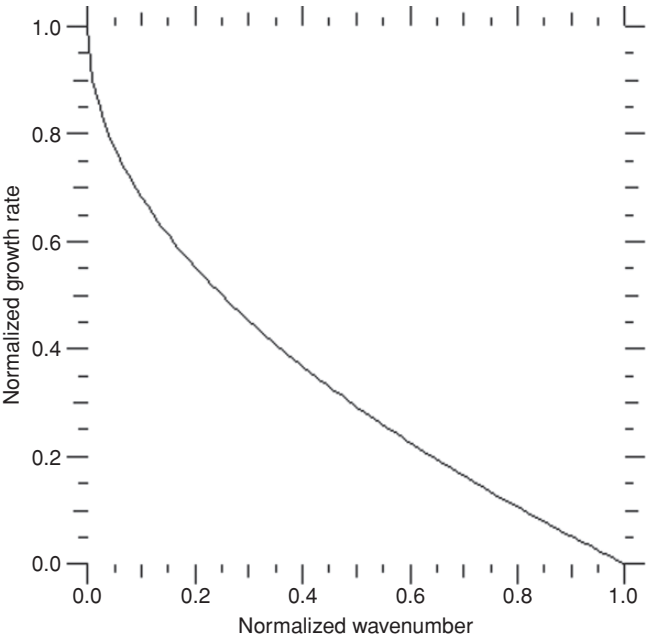


Figure 4.8 The normalized ablation-stabilized RT instability growth rate $\gamma_a/\gamma$ versus normalized wavenumber $k/k_c$, with $k_c$ the cutoff wavenumber defined in equation (4.66).

Note also from equations (4.66) and (4.67) that there is an advantage in having a cutoff wavenumber as low as possible. One way to achieve that is to have a high ablation velocity. The ablation velocity is basically the escape velocity of the plasma from a free surface. We saw in equation (4.49) that the escape velocity is directly proportional to the sound speed in the ablating plasma. The sound speed, in turn, is a function of the temperature, and hence the ablation pressure. We saw in Chapter 3 that we can get to higher ablation pressures at higher laser beam intensities. At these higher ablation pressures, however, the shell acceleration is also higher. So, once again, there is a tradeoff one must make among several parameters to find the right "goldilocks" implosion – not too fast, not too slow – that will remain stable throughout the motion.

Although the ablation process can provide some much-needed stabilization of RT instability growth at the outside surface of a laser-driven material, the opposite surface does not experience any ablation stabilization. At any interior interfaces that are accelerated or decelerated, the effects of RT growth of high wavenumbers can be significant. Small-scale surface roughness at these interfaces is important. We will say more about this in Section 4.3.4.

Finally, let us consider another important stabilization mechanism, viscosity. Since viscosity is the resistance to flow, kinematic viscosity $\nu$ (with units of length squared divided by time) can act to reduce substantially the growth of those perturbation wavelengths that are smaller than the characteristic scale of the viscosity, $\nu/u$.

If we were to include viscous forces in the equations of motion, then do a linearization similar to what we did in the previous subsection, we would find that we can write the following dispersion relation for the RT growth rate with viscosity:

$$\gamma_\nu^2 + 2k^2\nu\gamma_\nu - kAa = 0. \tag{4.68}$$

The solution of this second-order equation for the growth rate is

$$\gamma_\nu = k^2\nu\left\{\left[1 + \frac{Aa}{k^3\nu^2}\right]^{1/2} - 1\right\}. \tag{4.69}$$

Note from equation (4.69) that as $\nu \to 0$, $\gamma_\nu \to \sqrt{kAa}$; that is, in the limit of vanishing viscosity, the RT growth rate becomes equal to the classical RT growth rate, as it should. Note also that viscosity behaves more like a density gradient than like ablation in reducing the growth below classical. Thus, all modes are unstable; there is no cutoff wavenumber beyond which the growth is completely suppressed, but the growth is reduced more at higher wavenumbers. Growth vanishes entirely only for infinite wavenumber.

Let us define a characteristic wavenumber for viscosity-reduced RT growth,

$$k_c = \left(\frac{Aa}{\nu^2}\right)^{1/3}. \tag{4.70}$$

Using equation (4.70) we can rewrite equation (4.69) in terms of the normalized wavenumber:

$$\frac{\gamma_\nu}{\gamma} = \left(\frac{k}{k_c}\right)^{3/2}\left\{\left[1 + \frac{k_c^3}{k^3}\right]^{1/2} - 1\right\}. \tag{4.71}$$

Equation (4.71) is plotted in Figure 4.9. For wavenumbers $k < k_c$, there is only modest reduction in the classical growth rate of the instability because of viscosity. For $k > k_c$, there is much more reduction. At $k = k_c$, the RT growth rate is $\sqrt{2} - 1 \approx 0.41$ of the classical growth rate. Since the growth becomes negligibly small at high wavenumbers, we can define a cutoff wavenumber, just as we did for density-gradient-stabilized growth, beyond which we can ignore modeling

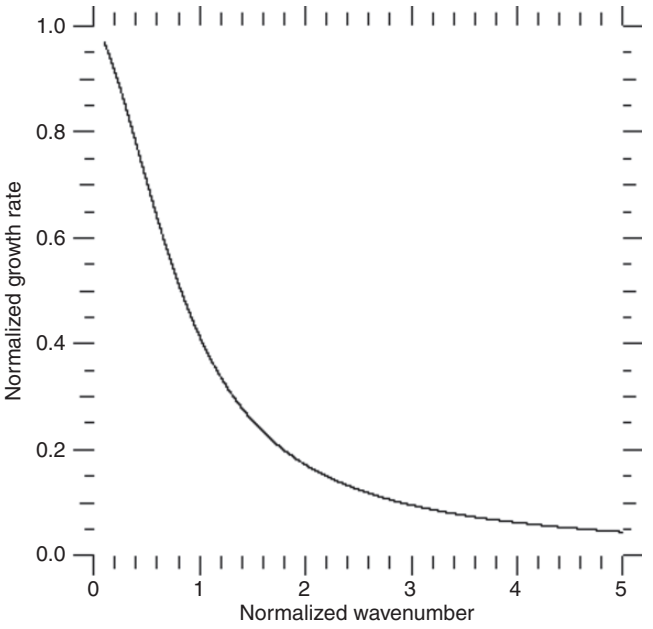


Figure 4.9 The normalized viscosity-stabilized RT instability growth rate $\gamma_v/\gamma$ versus normalized wavenumber $k/k_c$, with $k_c$ the characteristic wavenumber defined in equation (4.70).

the RT growth in a simulation. We will say more about this in Section 4.3.4 and in later chapters.

Before we discuss non-linear growth of the RT instability, and how the different modes couple non-linearly and then transition to turbulence, we first turn our attention briefly to two other hydrodynamic instabilities.

### *4.3.3 Kelvin–Helmholtz and Bell–Plesset*

Let us return to the picture in Figure 4.6, where we show schematically an interface separating two regions of different density, $\rho_2$ and $\rho_1$. The unperturbed interface is contained entirely in the $(x, y)$ plane. A small-amplitude perturbation, that is, a perturbation with amplitude $\eta \ll \lambda$, where $\lambda$ is the perturbation wavelength, initially grows in amplitude in the $z$-direction, that is, the direction perpendicular to the unperturbed interface.

Now let us consider that there is a shear flow at the interface. Thus, the fluid above the interface has a velocity in the $(x, y)$ plane different from the velocity of the fluid in the $(x, y)$ plane below the interface. In other words, there is a $z$-gradient in velocity at the interface. We can now make the same assumptions we made

https://doi.org/10.1017/CBO9781139095150.004 Published online by Cambridge University Press

above that allowed us to linearize the equations of motion from which we derived the growth rate of the RT instability. Unlike for the RT instability, however, where we were able to write the velocity, equation (4.50), as having a $z$-component that grows only exponentially in time, with shear flow, the $z$-component of velocity can either grow exponentially with time or it can oscillate. This is because all three coordinate directions influence the development of the motion – the direction of the gradients as well as the directions of **u** and **k**.

After doing the linearization and the algebraic manipulations as above, and finally applying the boundary conditions at the interface, we find that the growth rate of the single-mode perturbation at the interface, for the case where the interface separates two fluids of uniform density $\rho_2$ and $\rho_1$, is

$$\gamma = k\Delta u \frac{\sqrt{\rho_2 \rho_1}}{\rho_2 + \rho_1}. \tag{4.72}$$

Here, $\Delta u$ is the jump in shear velocity at the interface.

This instability is called the Kelvin–Helmholtz instability after the two nineteenth-century physicists who first independently considered it and derived the growth rate expression of equation (4.72). We will refer to the Kelvin–Helmholtz instability as the KH instability.

Note that, unlike for the RT instability, the KH growth rate is a maximum for a given mode number when the densities on either side of the interface are the same, that is, when $\rho_2 = \rho_1$. The maximum KH instability growth rate is then $\gamma_{\max} = k\Delta u/2$. When $\rho_2 \gg \rho_1$, the KH instability growth rate is much less,

$$\gamma = 2\gamma_{\max}\sqrt{\frac{\rho_1}{\rho_2}}. \tag{4.73}$$

Another important difference between the Kelvin–Helmholtz and the Rayleigh–Taylor instabilities is that any perturbation is Kelvin–Helmholtz unstable regardless of the direction of the acceleration. In other words, the perturbation grows whether $\rho_2 > \rho_1$ or $\rho_1 > \rho_2$, even when $\rho_2 = \rho_1$. It is the shear flow that drives the instability growth, not a pressure gradient in the direction opposite a density gradient as for RT.

In general, both instabilities may be operative at a density or material interface in flowing plasma. The overall instability growth rate can then be written as

$$\gamma = \frac{\left[k^2 (\Delta u)^2 \rho_1 \rho_2 + ak\left(\rho_2^2 - \rho_1^2\right)\right]^{1/2}}{(\rho_2 + \rho_1)}. \tag{4.74}$$

As we discussed above, there are different regions of instability growth depending on the magnitude and direction of the density gradient, and the magnitude of the shear velocity jump.

We emphasize again that the growth rates we have written for these instabilities describe the perturbation growth only for the initial phases of the growth, when the perturbation amplitude is less than the wavelength. This is because we derived these growth rates by linearizing the equations of motion. In doing this linearization, we neglected the non-linear terms in the equations. As the perturbation amplitude approaches in dimension the wavelength, the linear approximation breaks down. Then, we can no longer ignore the non-linear terms in the equations of motion. One effect of the non-linear terms is to generate harmonics of the wavenumbers that are initially present, and the coupling of these separate wavenumbers to create new modes that are beat frequencies of the original mode spectrum. In general we cannot find analytic solutions to the non-linear equations of motion, so we rely on computer simulations, which we discuss in more detail in later chapters. In the computer simulations, we can also treat more complex situations, such as fluids or plasmas in which there is not a uniform density on either side of the interface, and where there may be several stabilizing mechanisms at work, as well as a spectrum of initial mode numbers. This spectrum may be characteristic of the initial roughness of the interface, or it could be a mode spectrum that is set up by external forces driving the flow non-uniformly.

There are some situations, however, in which we can obtain approximate analytic solutions that include a changing wavenumber spectrum as the flow proceeds. One such situation is weakly non-linear RT growth in the presence of a spectrum of initial modes, which we consider in the next subsection. The other arises from the geometrical effects of spherical convergence, giving rise to the Bell–Plesset instability, which we hereinafter refer to as the BP instability.

The BP instability is identical to what is sometimes called the crenulation instability. Imagine a sinusoidal perturbation of wavelength $\lambda$ on the surface of a spherical shell of outer radius $r$. This perturbation is a crenulation of the surface. As the shell implodes under the action of some external driving force – laser ablation pressure, for example – the shell radius decreases. As a result of mass conservation, and assuming the shell is incompressible, this single-mode perturbation of mode number $\ell = 2\pi r/\lambda$ must decrease in wavelength as the radius decreases such that $\ell$ remains constant during the linear phase of the instability growth. Thus, $\lambda$ is directly proportional to $r$, and decreases as $r$ decreases. This is a purely geometrical effect, independent of whether or not the material is compressible.

Let us consider a spherical boundary between two fluids or plasmas of density $\rho_2$ and $\rho_1$, with the fluid "2" being the fluid exterior to the spherical boundary, which is initially at radius $r = r_0$. Let us also consider that the spherical boundary has a sinusoidal perturbation on it with mode number $\ell$ and initial amplitude $\eta_0 \ll r_0$. Using a velocity potential formulation, P. Amendt and co-workers in 2003 derived an equation for the perturbation amplitude growth during spherical convergence of

the spherical interface:

$$\ddot{\eta} + \frac{\dot{\eta}\dot{r}}{r}(3-\alpha)\beta_\ell - \frac{\eta}{r}[\ddot{r}\{A_\ell(\ell-1)+\alpha\beta_\ell\} + \dot{\alpha}\dot{r}\beta_\ell] = 0. \tag{4.75}$$

Here,

$$\alpha = -\frac{r}{\dot{r}}\frac{\dot{\rho}_2}{\rho_2} \tag{4.76}$$

is a dimensionless compressibility parameter,

$$\beta_\ell = \frac{\ell\rho_2}{\ell\rho_2 + (\ell+1)\rho_1}, \tag{4.77}$$

and

$$A_\ell = \frac{\ell\rho_2 - (\ell+1)\rho_1}{\ell\rho_2 + (\ell+1)\rho_1} \tag{4.78}$$

is a modal Atwood number at the interface. The second term on the left-hand side of equation (4.75) is the BP term and the third is the RT term.

Ignoring the RT term, we can write the solution of equation (4.75) as

$$\dot{\eta} \propto r^{\beta(\alpha-3)}. \tag{4.79}$$

Here both $\alpha$ and $\beta$ are assumed constant. For incompressible flow, $\alpha = 0$. Taking $\beta = 1$, equation (4.79) gives

$$\dot{\eta} \propto \frac{1}{r^3} \quad \text{or} \quad \eta \propto \frac{1}{r^2} \tag{4.80}$$

for constant velocity. Thus, the BP instability is a purely geometrical effect. Its effect is to enhance the perturbation amplitude as the spherical interface converges.

Note also from equation (4.75) that for compressible flow, for which $\alpha > 1$, there is less growth than for the incompressible case. For $\alpha = 2$ to 3, the effects of compressibility mostly cancel the effects of spherical convergence.

Even for compressible converging flow, for which the effects of the BP instability are small in contributing to the perturbation growth, we are left with the problem of an increasing wavenumber of the radially converging perturbation. As we have seen, for both RT and KH instabilities, in the absence of stabilization mechanisms, the instability growth rate increases as the wavenumber increases, and numerical schemes for solving the equations of motion, as we will see in later chapters, become unstable as the wavenumber increases.

### 4.3.4 Non-linear growth and turbulence

Until now, we have considered only the initial linear stages of hydrodynamic instability growth. The linear stage of instability growth takes place when the perturbation amplitude $\eta$ is small compared to the wavelength of the perturbation, that is, $\eta < \lambda$. When $\eta$ grows to become comparable to $\lambda$, then the assumptions we made in linearizing the equations of motion are no longer valid. We can no longer ignore the non-linear terms in the equations of motion. Once the perturbation growth enters its non-linear phase, we must typically solve simultaneously the whole set of partial differential equations describing the motion. As we already mentioned, in general we cannot find analytic solutions to these equations, but must instead apply numerical schemes to solve the equations. These direct numerical simulation, or DNS, schemes, however, can be fraught with their own difficulties and instabilities, which we will discuss in later chapters.

There are two other approaches to treating non-linear instability growth, though, that we briefly introduce here. We emphasize that this has remained a very active area of physics and mathematics research. In the search for understanding of non-linear physical phenomenology, whole new physical theories have developed over the last few decades, including chaos theory and turbulence theory. Whole new areas of mathematics have been developed, most notably fractal geometry. Books and journals on chaos theory, turbulence theory, fractal geometry, and non-linearities in physics have emerged, and even college courses. The brief discussion we present here is not meant in any way to summarize the vast literature and new understandings of non-linear phenomenology that have developed over the past few decades. Instead, we simply introduce the student to the importance of non-linearities in understanding the properties and behavior of matter at extreme conditions, and introduce two approaches that have been adapted to simulating non-linear instability growth in dense plasmas.

One approach follows from the recognition by S. Haan in 1989 that, largely because of ablative stabilization, perturbation growth at the ablation front of an imploding spherical shell that is driven by ablation pressure becomes and stays only weakly non-linear. This is because the shorter wavelength modes grow faster, reach the non-linear stage before the longer-wavelength modes do, and then these small bubbles essentially get "swallowed" by the larger ones, which continue to grow linearly until they reach their saturation amplitude, after which they get swallowed by even bigger bubbles, and so on. In the language of mathematics, modes with wavenumbers $k_2$ and $k_1$ couple, creating a new mode with wavenumber $k_2 - k_1$. Thus, in the presence of a spectrum of initial mode numbers, one can apply some amplitude saturation criterion that is dependent on the mode number, and then add

the individual mode amplitudes in quadrature to obtain an approximation of the total perturbation amplitude.

In Haan's scheme, then, we start with a set of calculations or simulations of the linear growth factors, $G_\ell$, of the individual modes. The linear-growth amplitudes of the individual modes are then $\eta_\ell = G_\ell \eta_{\ell 0}$, where $\eta_{\ell 0}$ is the initial amplitude of mode number $\ell$. These amplitudes, of course, are time-dependent. Then, we define the mode-saturation amplitude

$$\eta_{\ell,sat} = \frac{2r}{\ell^2}. \tag{4.81}$$

Since the radius $r$ is a function of time, so is the mode-saturation amplitude. The saturated or non-linear growth amplitude of mode number $\ell$ is then defined as

$$s_\ell = \min\left(\eta_{\ell,sat}, \eta_\ell\right)\left[1 + \log\frac{\max\left(\eta_{\ell,sat}, \eta_\ell\right)}{\eta_{\ell,sat}}\right]. \tag{4.82}$$

The individual mode amplitudes are then added according to the following prescription:

$$\sigma_{sat} = \sqrt{\frac{1}{2\pi}\sum_\ell s_\ell\,(2\ell+1)}\,. \tag{4.83}$$

The bubble amplitude is equal to $\sigma_{sat}$, and the spike amplitude is equal to $(1 + A)$ times the bubble amplitude, where $A$ is the Atwood number, given by equation (4.63). Note that the spike amplitude is always larger than the bubble amplitude, except in the symmetric case where the densities on either side of the unstable interface are the same.

This prescription for calculating non-linear multi-mode instability growth in ablatively driven spherical capsules is not predictive, but it is useful in obtaining reasonable estimates of expected instability growth. One must keep in mind, however, that this prescription has limited applicability: it can only work for those hydrodynamic instabilities that are only weakly non-linear.

For fully non-linear hydrodynamic instability growth, the flow becomes fully turbulent as a result of the non-linear mode coupling. What may start as pure linear RT instability growth becomes both RT and KH growth, as the denser material steepens and narrows into spikes and the less-dense material forms into buoyantly rising bubbles. Shear flows then cause the spike tips to roll over and curl up, while the bubbles form into rotating toroids. The two interpenetrating fluids or plasmas can then become completely mixed on the atomic scale as the non-linear flow transitions to fully turbulent flow. The width of this turbulent layer or mix layer, $\Delta h$ – which is essentially the sum of the lengths of the bubble and spike

amplitudes – no longer grows exponentially with time, as it did in the linear-growth stage. Instead, it grows dynamically as it is accelerated at acceleration $a$ as

$$\Delta h = \alpha a t^2, \tag{4.84}$$

where $\alpha$ is a constant. Experiments performed with many of the experimental devices described in Chapter 1 have all shown that the constant $\alpha \approx 0.07$. There may be some variation around this value of $\alpha$ depending on the Atwood number, but this general prescription for the growth of a turbulent mix layer seems to provide a result that is in reasonable agreement with experiment for a wide range of turbulent fluids and plasmas.

The success of such a simple prescription for characterizing the growth of a turbulent mix layer in non-linear hydrodynamic flow suggests an alternative to direct numerical simulation of such flow. In direct numerical simulation we must solve the non-linear equations of motion numerically for all the individual modes, which means that the computational mesh has to be fine enough to resolve the smallest-wavelength mode, because that is the mode that grows the fastest, and the first to reach non-linearity. To resolve a mode we typically want to specify several spatial points along the wavelength of the mode, so in order to follow the non-linear development of a multi-mode hydrodynamic instability, we must have computational grid sizes that are small compared to the smallest-wavelength mode number we are trying to follow. Not only can such a computation be prohibitively expensive and time-consuming, but, as we shall see in later chapters, very small grid sizes can lead to numerical instabilities that make the computational scheme unstable.

Instead of trying to resolve all the modes in the simulation, we can incorporate a "subgrid" model into the computation. In such a computation, we use our usual numerical scheme to solve the equations of motion for the bulk flow, and then at every time step in the computation we invoke a formula, like the one in equation (4.84), to describe what is happening on the subgrid scale. The dependent variables of the flow are then modified in those regions of the flow that are affected by the subgrid physics, and then the computation proceeds to the next time step. We go into much more detail on how all this is done in Chapters 11 and 12.

## 4.4 Example problems and exercises

In doing these problems and exercises, the student can use the thermodynamic and material properties for select materials listed in Appendix III.

**Exercise 4.1.** What is the momentum flux in a one-tenth solid density Al plasma that is flowing at a velocity one-tenth that of the solid-Al acoustic velocity?

https://doi.org/10.1017/CBO9781139095150.004 Published online by Cambridge University Press

**Exercise 4.2.** Write the generalized Navier–Stokes equations – equations (4.10), (4.11), and (4.12) – in cylindrical coordinates $r, \theta, \phi$.

**Exercise 4.3.** Derive the conservation of mass equation, equation (4.10), by integrating the zeroth moment of the Boltzmann equation with no external force term.

**Exercise 4.4.** Derive the conservation of momentum equation, equation (4.11), by integrating the first moment of the Boltzmann equation with no external force term.

**Exercise 4.5.** Derive the conservation of energy equation, equation (4.12), by integrating the second moment of the Boltzmann equation with no external force term.

**Exercise 4.6.** Use equations (4.10) and (4.14) to show that, for incompressible flow, the streamline function $\psi$ is constant in the direction of the velocity vector.

**Exercise 4.7.** Vorticity develops when any fluid or plasma bubble buoyantly rises, or flows through a surrounding fluid or plasma that is cooler and denser. For a buoyantly rising bubble in a uniform, compressible medium, Hill spherical vortex theory predicts that the circulation $\Gamma$ is constant, that is,

$$\Gamma = \int \nabla \times \mathbf{u} \cdot d\mathbf{S} = \oint \mathbf{u} \cdot d\mathbf{l} = 5 \left( \frac{\rho}{\rho_0} \right)^{1/3} va = \text{constant},$$

where $v$ is the vortex rise rate and $a$ its radius. Hill spherical vortex theory is valid for $a \ll Z - Z_0$, where $Z - Z_0$ is the height of the bubble rise. Show that (i) for a vortex ring, in which vorticity is confined to the bubble edge and $a \propto \exp(Z)$, then $a \propto t$, $v \propto 1/t$; and that (ii) for a vortex bubble, in which vorticity is uniform throughout the volume of the bubble and $a \propto Z$, then $a \propto t^{1/2}$, $v \propto t^{-1/2}$.

**Exercise 4.8.** Show from Poisson's equation, equation (4.15), that in planar Couette flow, the horizontal velocity component, $u_x$, is a linear function of the $y$-coordinate; that is,

$$u_x = u_0 + (v - u_0) \frac{y}{L},$$

where $u_0$ is the velocity at the bottom plate, $v$ the velocity at the top plate, and $L$ is the distance between the plates.

**Exercise 4.9.** Write the equivalent 3D versions of the 1D versions of the Lagrangian formulation of the Navier–Stokes equations, equations (4.23), (4.24), and (4.25).

**Exercise 4.10.** Show that the equations of motion in cylindrical coordinates are *not* invariant under linear transformation of the independent variables.

**Exercise 4.11.** Let us consider plasma in which the pressure $P$ is not directly proportional to its density $\rho$, and another plasma with an identical relation between pressure and density (i.e., an identical equation of state) but with a pressure scaled by a multiplicative factor $s_P$ and density scaled by a different multiplicative factor $s_\rho$. Show that the two plasmas are hydrodynamically self-similar if the spatial and temporal scalings are selected so that

$$s_x = s_t \sqrt{\frac{s_\rho}{s_P}}.$$

**Exercise 4.12.** Draw the characteristic curves for the one-dimensional compression wave illustrated schematically in Figure 4.3.

**Exercise 4.13.** How far into a solid Al slab does a 100-kbar compression wave travel in 20 ns? To what density is the Al slab compressed by this compression wave?

**Exercise 4.14.** What is the escape velocity of air at STP? How does this velocity compare to the STP thermal velocity of oxygen and nitrogen molecules? What is the escape velocity of hydrogen? How does this escape velocity compare to the STP thermal velocity of hydrogen molecules?

**Exercise 4.15.** Consider a 1-cm$^3$ volume of one-tenth-solid density Al plasma being accelerated by a 1-Mbar pressure pulse of 20-ns duration. What is the classical Rayleigh–Taylor growth rate of a 1-μm amplitude, 20-μm wavelength sinusoidal perturbation on the surface of this plasma? How much time passes before the perturbation growth starts to become non-linear?

**Exercise 4.16.** If, for the plasma described in Exercise 4.15 above, there is a density-gradient scale length at the plasma surface equal to the perturbation wavelength, by how much is the classical Rayleigh–Taylor growth rate reduced?

**Exercise 4.17.** If the plasma described in Exercise 4.15 above has a viscosity of $10^4$ cm$^2$ s$^{-1}$ (approximately the viscosity of cold cream – glycerin), by how much is the classical Rayleigh–Taylor growth rate reduced?

**Exercise 4.18.** Consider one-tenth-solid density Al plasma flowing past one-tenth-solid density Fe plasma at relative velocity $10^6$ cm s$^{-1}$. What is the classical Kelvin–Helmholtz growth rate of a 1-μm amplitude, 20-μm wavelength sinusoidal perturbation on the interface between these two plasmas? How much time passes before the perturbation growth starts to become non-linear?

**Exercise 4.19.** Consider a spectrum of perturbation modes on the surface of a spherical shell of initial radius 1 mm that is imploding at constant acceleration. All

the modes have initial amplitude 0.1 μm. If mode number 30 has grown by a factor of ten at the time it reaches its saturation amplitude, at what shell radius does this mode number reach saturation?

**Exercise 4.20.** Read the 2000 paper by Dimonte listed in the Further Reading. According to this work, how is the "constant" $\alpha$ in equation (4.84) dependent on Atwood number? Is the growth of the mix layer symmetric on both sides of the initial interface? If not, how is it different?